BIOCHEMISTRY
including biophysical chemistry & molecular biology

Article

pubs.acs.org/biochemistry

On the Role of the Appended P19 Element in Type A RNAs of Bacterial RNase P

Vassiliki Stamatopoulou,[†] Chrisavgi Toumpeki,[†] Anastassios Vourekas,[†,∥] Maria Bikou,[†] Marianthi Tsitlaidou,[†] Andreas G. Tzakos,[‡] Amalia Afendra,*[,§] Constantin Drainas,[‡] and Denis Drainas*[,†]

[†]Department of Biochemistry, School of Medicine, University of Patras, Patras, Greece

[‡]Department of Chemistry, Sector of Organic Chemistry and Biochemistry, University of Ioannina, Ipiros, Greece

[§]Department of Biological Applications and Technologies, University of Ioannina, Ipiros, Greece

Supporting Information

ABSTRACT: Comparative *in silico* analyses of bacterial RNase P enzymes clustered their RNA subunits in type A RNA, found in *Escherichia coli*, and in type B, found in *Bacillus subtilis*. *Zymomonas mobilis* RNase P consists of one protein (*Zmo*-RnpA) and one type A RNA (RPR) subunit containing the P19 element, present in many RNase P RNAs of any structure class but lacking in the *E. coli* RNase P RNA. To investigate the putative role of the P19 stem, we constructed a P19 deletion RNA mutant (ΔP19RPR) and performed detailed kinetic analysis of reconstituted enzymes in the presence of the homologous *Zmo*-RnpA protein or *Eco*-RnpA protein from *E. coli*. The deletion of P19 perturbs the monovalent ion requirements. The Mg^{2+} requirement for the ΔP19RPR holoenzyme was almost identical to that for the wtRPR holoenzyme at Mg^{2+} concentrations of ≤25 mM. Interestingly, enzymes reconstituted with *Eco*-RnpA protein, relative to those assembled with *Zmo*-RnpA, exhibited enhanced activity in the presence of ΔP19RPR, suggesting that *Eco*-RnpA protein can effectively replace its *Z. mobilis* counterpart. Homologous and heterologous reconstituted enzymes in the presence of ΔP19RPR exhibited differences in their K_m values and catalytic efficacies. Overall, the presence of the P19 stem points toward an adaption during the co-evolution of *Zmo*-RnpA and RPR that is essential for stabilizing the overall structure of the *Z. mobilis* RNase P. Finally, our results are in line with existing structural data on RNase P enzymes and provide biochemical support for the possible role of appended domains in RNase P RNA subunits.

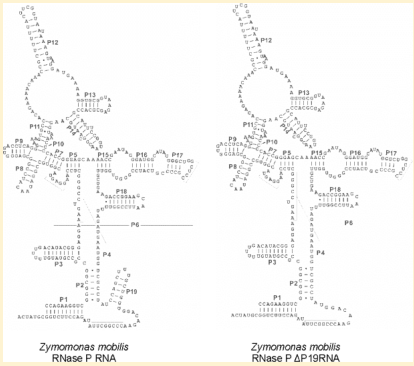

Ribonuclease P (RNase P) is an essential ribonucleoprotein complex that cleaves the 5′-leader sequence of precursor tRNAs (pre-tRNAs) during their biogenesis.[1] Almost all forms of RNase P, with a few recent exceptions,[2−4] contain a single RNA subunit (RPR) and one (in bacteria) or more (in archaea and eukaryotes) protein subunits.[5]

Two distinct types of catalytic RNA subunits of RNase P that were originally characterized from *Escherichia coli* (type A, the most ancestral and abundant form) and *Bacillus subtilis* (type B) exist. Despite their different topologies and proposed secondary structures, both types can form functional holoenzymes *in vitro* with heterologous protein subunits from bacteria expressing the other type of P RNA.[1] Moreover, adequate studies support the notion that the structural differences between the two types of RNA reflect the different biochemical idiosyncrasies of the RNA subunits, their different origin, and ultimately the differences in the *in vitro* activities. Nevertheless, it was shown recently that type A and type B RNAs are interchangeable *in vivo* despite substantial biophysical differences.[6]

Furthermore, the differences between the two RPR structural types seem to be species-specific and might represent the possible alternative roles of RNase P besides its prominent role in tRNA maturation. Such an example was reported recently with the discovery of a minimal form of the RNase P form of the RNA subunit (termed type T) in the archaeal *Pyrobaculum* species. This minimal RNA subunit lacks the specificity domain, suggesting that this structural peculiarity is associated with alternative functions of the ribozyme such as small RNA processing.[7] The functions of specific structural elements, which are absent in the type A or type B forms, remain elusive, for most cases, and only few studies have addressed their function. It was recently shown that insertion of the P15−P17 domain from *E. coli* into the human RNA subunit (H1 RNA), which has very low RNA-alone activity, did not improve the cleavage activity despite the essential role of the P15 domain in the binding site of the 3′-CCA end of tRNAs. Surprisingly, the P15 loop module itself was still able to cleave pre-tRNA substrates at the canonical site, although at very low rates, when separated from the full-length RPR, as part of small chimeric RNA molecules.[8]

To provide more insight into the role of these structural differences, we performed bioinformatics analyses and focused

Received: August 13, 2013
Revised: February 28, 2014
Published: February 28, 2014

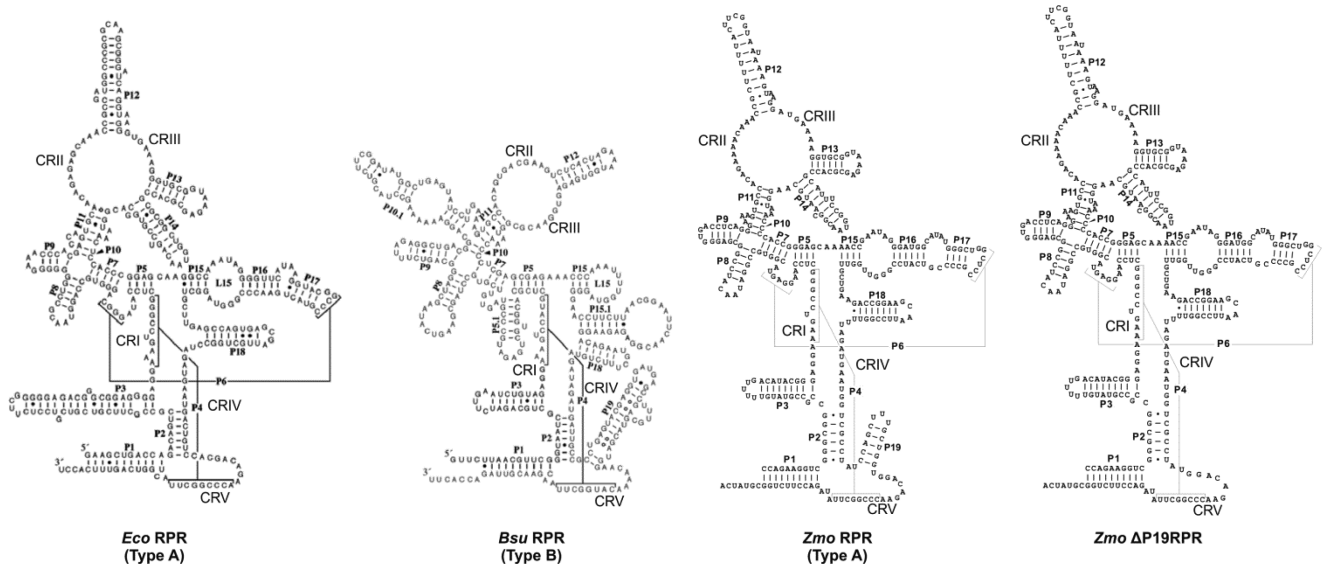

Figure 1. Secondary structures of *Z. mobilis* RNase P wild-type (*Zmo* wtRPR) or ΔP19 (*Zmo* ΔP19RPR) RNA subunits, in comparison with the secondary structure of the type A *E. coli* RNase P RNA subunit (*Eco* RPR) and the type B *B. subtilis* RNase P RNA subunit (*Bsu* RPR).

on the P19 element, a phylogenetically unstable structure, present in many RNase P RNAs of any structural class, but lacking in the *E. coli* RNase P RNA (Figure 1).[9] On the basis of this observation, we cloned the subunits and characterized the RNase P holoenzyme from the ethanol-producing anaerobic Gram-negative *Zymomonas mobilis*.[10] The holoenzyme exhibited an ionic concentration requirement similar to those of other known RNase Ps, albeit it was slightly elevated with respect to those of Mg^{2+} and monovalent ions. *Z. mobilis* has rather a small genome (2056 kb, almost half the size of that of *E. coli*), encoding an RNase P RNA subunit of type A, which, however, has acquired a well-defined P19 element of 13 nucleotides. To shed light on the possible roles and biochemical and biophysical properties of this element as well as its effect on the overall behavior of the holoenzyme, we constructed a P19 deletion RNA mutant, which was used for subsequent biochemical analysis. After estimating the kinetic constants of the holoenzyme and its RNA subunit, we observed that the absence of the P19 stem does not significantly affect the requirement for Mg^{2+} in the lower concentration range ($\leq$25 mM) but increases the requirement for monovalent ions. Moreover, the sequence alignment of *Zmo*-RnpA with other RNase P proteins (RPPs) derived from holoenzymes with type A RNAs lacking the P19 element revealed that specific conserved amino acid residues are changed in *Zmo*-RnpA. In addition, *Zmo*-RnpA carries an N-terminal extension of approximately 40 amino acids relative to *E. coli* RnpA (*Eco*-RnpA).

To further explore the functional role of the P19 stem–loop, we conducted heterologous reconstitution experiments in which the *Zmo*-RnpA protein was replaced with the *Eco*-RnpA protein. It was found that *Eco*-RnpA could improve the bimolecular rate constant (k_{cat}/K_m) of ΔP19RPR when its cognate protein failed to do so. This observation could be due to elimination of specific contact points between mutant RPR and cognate protein due to P19 deletion or the fact that *Eco*-RnpA contains more residues capable of forming contacts (or an equal number of residues forming stronger contacts) with the RPR that better compensate for the destabilizing effect of the P19 depletion. Overall, this study improves our understanding of evolution of RNA–protein cofunction in RNase P enzymes of different origin.

MATERIALS AND METHODS

RNase P Purification and Assay for RNase P Activity. *Z. mobilis* cells (strain ATCC10988 wild type) were grown at 30 °C, without being shaken in Zymo Broth medium,[11] which contains 2% (w/v) glucose, 0.1% (w/v) $(NH_4)_2SO_4$, 0.1% (w/v) KH_2PO_4, 0.04% (w/v) $MgSO_4$, and 0.5% (w/v) yeast extract. Cells were disrupted in a buffer containing 10 mM $MgCl_2$, 10% (v/v) glycerol, 10 mM β-mercaptoethanol, 1 mM PMSF, 50 mM Tris-HCl (pH 8.0), and 50 mM KCl by sonication, and the production of the S-100 fraction was conducted as previously described.[12] The purification procedure consisting of two subsequent steps of anion exchange chromatography (DE-52 cellulose) was conducted as previously described.[13] Enzyme assays were conducted at 37 °C in 20 μL of buffer Z [25 mM $MgCl_2$, 50 mM NH_4Cl, 50 mM Tris-HCl (pH 8), and 1 mM β-ETSH] in the presence of 5 fmol of labeled transcript of the *Schizosaccharomyces pombe* pre-tRNA^{Ser} gene (pSupS1) and 1.3 μg of protein from the RNase P fraction. The reactions were quenched by the addition of 5 μL of stop dye (80% formamide, 50 mM EDTA, 0.1% bromophenol blue, and 0.1% xylene cyanol). Reaction products were analyzed on 10% polyacrylamide–8 M urea gels. Throughout this work, the Phosphorimager Fujifilm FLA 3000 and AIDA software were used for the visualization and quantification of radioactive signals.

Modeling of wtRPR and ΔP19RPR. The RNase P RNA of *Z. mobilis* was built through comparative modeling using ModeRNA[14] and assemble (reference, PMID 20562414). The three-dimensional (3D) structural model of the target RNA sequence was obtained by using as a structural template the *Thermotoga maritima* RNase P RNA in the presence of tRNA, a postcleavage tRNA leader, P protein, and Mg^{2+}.[15] P19 stem comparative modeling was performed on the basis of the P19 stem of the crystal structure of the *Bacillus stearothermophilus* RNase P RNA.[16] The electrostatic potential surface was calculated with the PBEQ Solver of CHARMM and visualized with PyMOL. Bounds for electrostatic potential map visual-

dx.doi.org/10.1021/bi4011013 | *Biochemistry* 2014, 53, 1810–1817

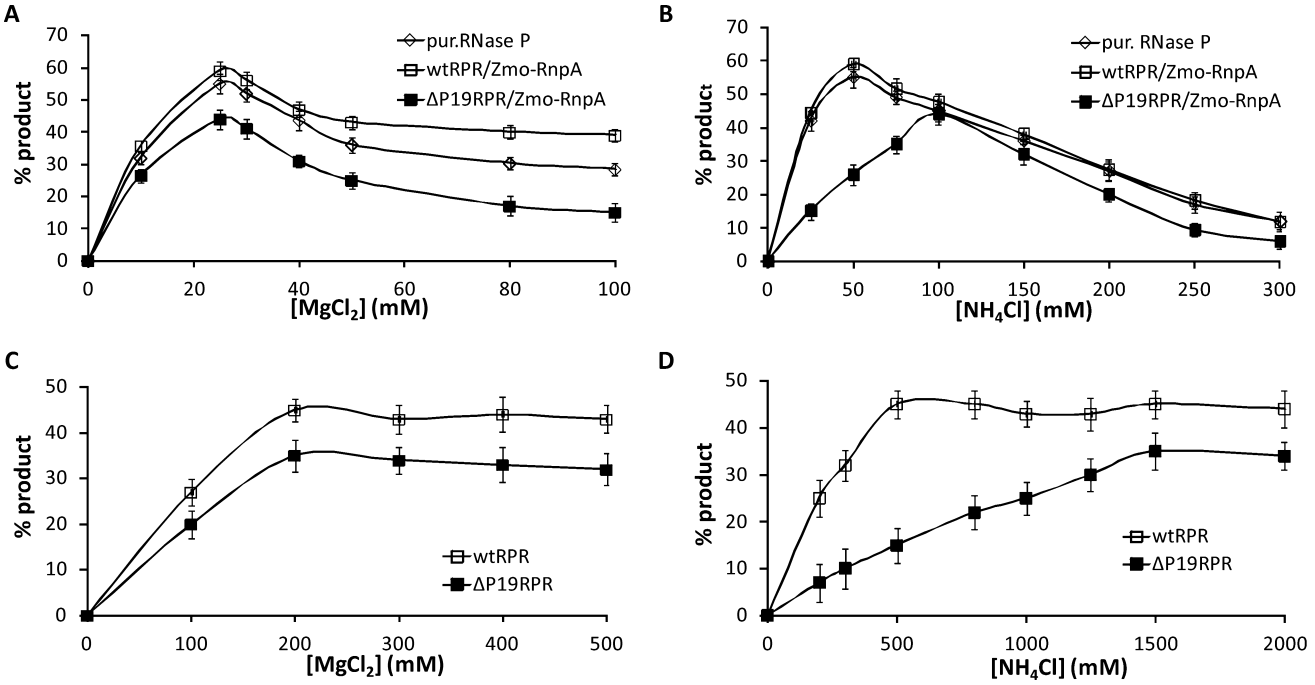

Figure 2. Screening of $MgCl_2$ and NH_4Cl concentration requirements for the *Z. mobilis* RNase P activity of the purified holoenzyme and the reconstituted forms (wtRPR/*Zmo*-RnpA or ΔP19RPR/*Zmo*-RnpA) (A and B) or the RPRs alone (C and D). The percent product was defined as the fraction of band intensities corresponding to the cleavage products (mature tRNA and 5′-leader) relative to those of all bands (i.e., the total amount of substrate added in each reaction mixture is considered as 100%). The $MgCl_2$ concentration for the purified enzyme and the holoenzymes reconstituted with wtRPR was varied at 50 mM NH_4Cl and for the reconstituted holoenzymes with ΔP19RPR at 100 mM NH_4Cl. The NH_4Cl concentration was varied in the presence of 25 mM $MgCl_2$ for all three types of holoenzymes. The $MgCl_2$ concentration was varied for wtRPR and ΔP19RPR in the presence of 500 and 1500 mM NH_4Cl, respectively, while the $MgCl_2$ concentration was kept at 200 mM for NH_4Cl concentration variation with both types of RPRs.

ization were set to ±2 kcal mol^{-1} e^{-1}. All RNA superpositions were performed with SARA.[17] To build the holoenzyme, the *Z. mobilis* protein was constructed independently through comparative modeling using Modeler[18] on the basis of the *T. maritima* P protein.[15] Protein electrostatic potential maps were calculated with MOLMOL.[19] The protein, tRNA, leader, and metal ions were docked onto the RNase P RNA using as a template the *T. maritima* RNase P holoenzyme crystal structure. To detect highly conserved positions in the protein structure, we used ConSurf.[20] The multiple-sequence alignment was built using MAFFT. The homologues were collected from UNIREF90. The homologue search algorithm was BLAST, with the PSI-BLAST *E*-value cutoff set to 0.0001. The maximal %ID between sequences was set to 95, and the minimal %ID for homologues was set to 35. The calculation method for conservation scores was Bayesian, and the model of substitution of proteins was JTT.

Kinetic Analysis of the Reconstituted RNase P Complexes and the RPRs. The *Zmo* wtRPR or the *Zmo* ΔP19RPR transcript (0.25 pmol of either) was preincubated for 20 min at 37 °C in 20 μL of reaction buffer containing 500 mM $MgCl_2$, 50 mM Tris-HCl (pH 8), and 800 mM (*Zmo* wtRPR) or 1500 mM NH_4Cl (*Zmo* ΔP19RPR). Bacterial RNase P holoenzyme activity was reconstituted by mixing 0.25 pmol of *Zmo* wtRPR or *Zmo* ΔP19RPR transcript and 2.5 pmol of purified RpnA protein for 10 min at 37 °C in 20 μL of reaction buffer Z containing 50 mM Tris-HCl (pH 8), 25 mM $MgCl_2$, and 50 mM (*Zmo* wtRPR) or 100 mM NH_4Cl (*Zmo* ΔP19RPR). Enzymatic reactions for the RPRs and the reconstituted holoenzymes were conducted for 1 min at 37 °C. Reaction rates were measured from the slopes of the time plots in the presence of labeled pSupS1 (1 nM) and various concentrations of unlabeled pSupS1 (50−250 nM) at 37 °C. The kinetic constants (K_m and k_{cat}) of enzymatic activities were calculated from the Michaelis−Menten diagrams by using the curve-fitting program Kaleidagraph. For each kinetic curve, at least three independent experiments were performed.

Mobility Shift Assay. The [α-^{32}P]GTP-labeled transcript of pSupS1 (0.05 pmol) was incubated with increasing amounts of the *Zmo* wtRPR or *Zmo* ΔP19RPR transcript (0.5, 1, 2, or 5 pmol) for 90 min at 30 °C. The reactions (20 μL) were conducted in 1× binding buffer [50 mM Tris-Cl (pH 8), 25 mM $Mg(OAc)_2$, and 100 mM NH_4OAc]. All the RNA molecules were heat denatured at 90 °C for 1 min and renatured on ice for 2 min. The RNA−RNA complexes were analyzed by electrophoresis on a 6% native polyacrylamide gel in 1×TB buffer (35 mM Tris base and 17.5 mM boric acid), containing 5 mM $MgCl_2$ and 5% glycerol, at 4 °C.

RESULTS

P19 Deletion Affects the Ammonium Requirements of RNase P. To study the role of the P19 stem−loop, we chose *Z. mobilis* (*Zmo*), a Gram-negative bacterium whose RPR secondary structure is clearly A type, similar to that of *E. coli*, bearing all the conserved features except for the additional 13-nucleotide P19 stem−loop (Figure 1). To address the question of whether the deletion of the P19 stem affects the ionic requirements of the RNase P holoenzyme, we cloned the annotated gene sequences of the RNase P protein (RnpA, gene *rnpA*) and RNA (RPR, gene *rnpB*) subunits from *Z. mobilis* (gene IDs 12281968 and 12281311, respectively)[21] (see the

dx.doi.org/10.1021/bi4011013 | *Biochemistry* 2014, 53, 1810−1817

Supporting Information). The *Zmo-rnpA* ORF encodes a positively charged protein (pI 11.16), consisting of 154 amino acid residues with a calculated molecular mass of 17.23 kDa. The *Zmo* RPR gene encodes a 375-base RNA, with a sequence that is 69% homologous with that of *E. coli* (*Eco*) RPR. On the basis of the *Zmo* RPR sequence, we constructed a mutant *Zmo* RPR, ΔP19RPR (see the Supporting Information), which lacks the P19 structural element (Figure 1). The recombinant *Zmo-rnpA*-His_6 was expressed in *E. coli*, and its purified native form was used in combination with the *in vitro* transcribed *Zmo* RPR or ΔP19RPR for reconstitution experiments. Additionally, the native RNase P enzyme was purified from the S-100 fraction of *Zmo* cell extracts by DEAE-cellulose chromatography and was analyzed in enzymatic assays, as well.

pH and temperature optima for the purified and the reconstituted RNase P, as well as for the *Zmo* wtRPR and ΔP19RPR, were found to be 8 and 37 °C, respectively. Moreover, the purified and reconstituted holoenzyme forms of *Zmo* RNase P were determined to require 25 mM $MgCl_2$ and 50 mM NH_4Cl for optimal activity at pH 8 and 37 °C (Figure 2A,B). In comparison, the *Zmo* RPR ribozyme requires 200 mM Mg^{2+} and 800 mM NH_4^+ for maximal activity under otherwise identical conditions (Figure 2C,D). On the other hand, enzymatic assays with ΔP19RPR revealed the optimal activity at 200 mM $MgCl_2$ and 1500 mM NH_4Cl (Figure 2C,D). Thus, removal of P19 seems not to affect concentration requirements for Mg^{2+} but increases the requirement for NH_4^+ from 0.8 to 1.5 M (Figure 2C,D). In addition, when ΔP19RPR was mixed with *Zmo*-RnpA, in a proportion of 1:10, the reconstituted holoenzyme displayed optimal activity at 25 mM $MgCl_2$ and 100 mM NH_4Cl. It is worth noting that the concentration of NH_4^+ ions needed for optimal activity of the *Zmo* mutant holoenzyme is 2-fold higher than that required for the *Zmo* wt holoenzyme. All assays were performed using pSupS1 as the substrate.

Deletion of the P19 Stem Does Not Affect the Binding Affinity of RPR for the Substrate. In an attempt to address whether the P19 stem deletion affects the binding affinity of the pSupS1 substrate for *Zmo* ΔP19RPR, electromobility shift assays were performed under conditions where *Zmo* wtRPR and *Zmo* ΔP19RPR have very low catalytic activity. Although only a minor fraction of substrate could be shifted into gel-resolvable complexes, quantification of the bands corresponding to free pSupS1 and the *Zmo* wtRPR−pSupS1 and *Zmo* ΔP19RPR−pSupS1 complexes was used to determine the $^{app}K_d$ values of RPRs for the substrate, providing evidence that deletion of P19 does not affect substrate binding (Figure 3, inset, lanes 2−5 and 6−9). The corresponding $^{app}K_d$ values of *Zmo* wtRPR ($^{app}K_d$ = 384 nM) and *Zmo* ΔP19RPR ($^{app}K_d$ = 390 nM) were calculated from the slopes of the Scatchard plots (Figure 3). This result is in accordance with the P19 hairpin not being at the RPR−substrate interface (Figure 1).

P19 Deletion Affects the Kinetic Constants of RNase P and RPR. Standard Michaelis−Menten kinetics were conducted for the reconstituted *Zmo* wtRPR−*Zmo*-RnpA and *Zmo* ΔP19RPR−*Zmo*-RnpA complexes and for *Zmo* wtRPR and *Zmo* ΔP19RPR alone (Figure 4A,B). The estimated K_m values for *Zmo* wtRPR and *Zmo* ΔP19RPR are identical (Table 1), which is in agreement with the binding data described above. Furthermore, the estimated k_{cat} values for *Zmo* wtRPR and *Zmo* ΔP19RPR are 2.7 and 0.7 min^{-1}, respectively (Table 1). Moreover, the K_m and k_{cat} values for the *Zmo* wtRPR−*Zmo*-RnpA holoenzyme are 120 nM and 4.7 min^{-1}, respectively, and

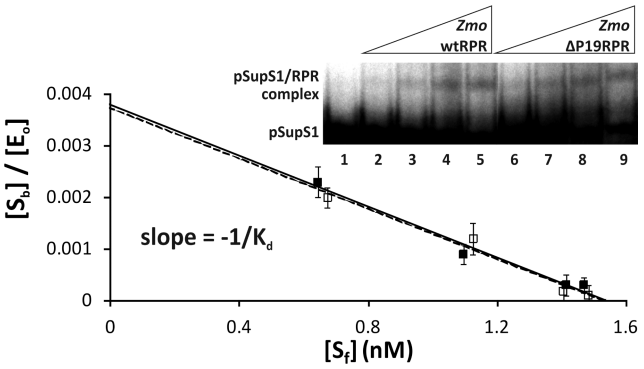

Figure 3. Scatchard plot for binding of the pSupS1 substrate to *Zmo* wtRPR or *Zmo* ΔP19RPR, where [Sf] is the substrate free concentration, [Sb] is the substrate-bound concentration, and [Eo] is the total enzyme concentration. Complexes were formed with a constant amount of substrate (1.5 nM) and excess amounts of *Zmo* wtRPR (◇) or *Zmo* ΔP19RPR (△), varying from 50 to 500 nM. $^{app}K_d$ values were determined from the reciprocal of the slopes of the lines. The inset shows the autoradiogram of a representative gel shift assay of the binding of the pSupS1 substrate to *Zmo* wtRPR or *Zmo* ΔP19RPR: lane 1, substrate alone; lanes 2−5, substrate incubated with increasing concentrations of *Zmo* wtRPR; lanes 6−9, substrate incubated with increasing concentrations of *Zmo* ΔP19RPR.

the K_m and k_{cat} values for the *Zmo* ΔP19RPR−*Zmo*-RnpA holoenzyme are 650 nM and 0.9 min^{-1}, respectively. Notably, the catalytic potency (k_{cat}/K_m) of the *Zmo* ΔP19RPR−*Zmo*-RnpA holoenzyme (1.4 min^{-1} μM^{-1}) is considerably decreased compared to that of the *Zmo* wtRPR−*Zmo*-RnpA holoenzyme (39 $min^{-1}\mu M^{-1}$) (Table 1). One possibility is that removal of the P19 hairpin perturbs the structure of the C-domain, leading to suboptimal interaction with *Zmo*-RnpA.

***Zmo*-RnpA Can Be Effectively Substituted with *Eco*-RnpA.** To further explore the functional role of P19, we conducted heterologous reconstitution experiments. The *Zmo*-RnpA protein was replaced with the *Eco*-RnpA protein, and the kinetic constants of the heterologous *Zmo* wtRPR−*Eco*-RnpA and *Zmo* ΔP19RPR−*Eco*-RnpA holoenzymes were determined (Figure 4A,B and Table 1). Surprisingly, K_m and k_{cat} values for the heterologous *Zmo* wtRPR−*Eco*-RnpA holoenzyme are slightly improved in comparison with the K_m and k_{cat} values for the homologous *Zmo* wtRPR−*Zmo*-RnpA holoenzyme (Table 1), showing that *Eco*-RnpA can effectively replace *Zmo*-RnpA, at least for pSupS1 processing. Even more strikingly, the heterologous *Zmo* ΔP19RPR−*Eco*-RnpA holoenzyme appears to be catalytically more efficient than the reconstituted homologous *Zmo* ΔP19RPR−*Zmo*-RnpA holoenzyme. The k_{cat}/K_m values for these two holoenzymes are 3.2 and 1.4 min^{-1} μM^{-1}, respectively (Table 1), revealing that *Eco*-RnpA improves the catalytic potency of the holoenzyme at least 2.3-fold relative to that of *Zmo*-RnpA. It is worth noting that homologous and heterologous holoenzymes reconstituted with *Zmo* wtRPR or ΔP19RPR revealed almost identical end points of their cleavage reactions (data not shown).

Modeling of *Zmo RPR* and *Zmo*-RnpA. The *Z. mobilis* RNase P holoenzyme and its mutant variant were modeled using as a template the crystal structure of the *T. maritima* RNase P RNA in the presence of tRNA, a postcleavage tRNA leader, P protein, and Mg^{2+} (Figure S1 of the Supporting Information; for the electrostatic surface plot, see Figure S2 of the Supporting Information).[15] The 3D architecture of the modeled *Zmo* RNase P as well as its superposition with the

dx.doi.org/10.1021/bi4011013 | *Biochemistry* 2014, 53, 1810−1817

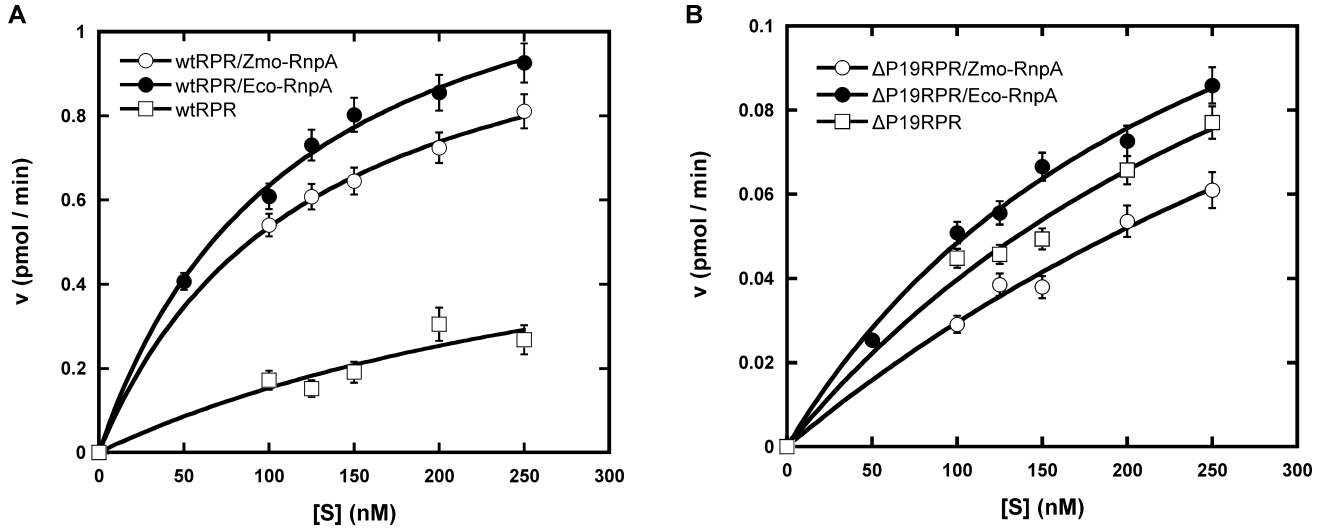

Figure 4. Kinetic analysis of reconstituted RNase P holoenzymes or *Z. mobilis* RPRs alone using the pSupS1 substrate. Michaelis–Menten diagrams of (A) *Zmo* wtRPR alone (wtRPR) and the reconstituted complexes with *Zmo*-RnpA or *Eco*-RnpA protein and (B) *Zmo* ΔP19RPR alone (ΔP19RPR) and the reconstituted complexes with *Zmo*-RnpA or *Eco*-RnpA protein. For reaction conditions, see the footnote of Table 1.

Table 1. Estimated Kinetic Parameters K_m, V_{max}, and k_{cat} and k_{cat}/K_m Ratio of *Zmo* RPRs Alone and Its Reconstituted Complexes

	K_m (nM)[a]	V_{max} (pmol/min)[a]	k_{cat} (min^{-1})	k_{cat}/K_m (min^{-1} μM^{-1})
Zmo wtRPR	380 ± 6	0.7 ± 0.05	2.7	7
Zmo ΔP19RPR	380 ± 8	0.2 ± 0.05	0.7	1.8
Zmo wtRPR–*Zmo*-RnpA	120 ± 3	1.2 ± 0.3	4.7	39
Zmo ΔP19RPR–*Zmo*-RnpA	650 ± 5	0.2 ± 0.04	0.9	1.4
Zmo wtRPR–*Eco*-RnpA	115 ± 5	1.4 ± 0.2	5.5	48
Zmo ΔP19RPR–*Eco*-RnpA	250 ± 8	0.2 ± 0.01	0.8	3.2

[a]The standard errors of the curve fits shown in Figure 4 are indicated in the estimates of K_m and V_{max}.*Zmo* wtRPR or *Zmo* ΔP19RPR was preincubated for 20 min at 37 °C in 200 mM $MgCl_2$, 50 mM Tris-HCl (pH 8), and 800 or 1500 mM NH_4Cl, respectively, and incubated after the addition of the substrate for 1 min at 37 °C. Homologous and heterologous RNase P holoenzymes were reconstituted by being preincubated for 10 min at 37 °C in 50 mM Tris-HCl (pH 8), 25 mM $MgCl_2$, and 50 or 100 mM NH_4Cl for *Zmo* wtRPR or *Zmo* ΔP19RPR, respectively, followed by the addition of substrate and incubation for 1 min at 37 °C.

Zmo ΔP19RPR mutant can be seen in Figure 5A. P19 is modeled as coaxially aligned and in the proximity of the P1 stem. The modeled *Zmo*-RnpA adopts an overall *αββββαβα* topology and is in contact with the *Zmo* RPR catalytic domain on one side of the P15 helix, the conserved regions CRIV and CRV, and the interfaces of helices P3 and P2. Domains of *Zmo*-RnpA that are of particular interest include the central cleft (that recruits and interacts with the 5′-leader of pre-tRNA) and the conserved RNR motif [residues 100–106 (Figure 5B)]. This motif is positioned close to the 5′-leader, the 3′-end of pre-tRNA, and also helices P2 and P4.[15] The RNR motif and residues adjacent to it (residues N96, R102, K104, R105, and R108) are in the proximity of RPR helices P2–P4 and P19 and conserved regions CRI, CRIV, and CRV. From the model, we can see that the relevant residues in *Z. mobilis* are located in important RPR sites. Specifically, R100 of the RNR motif is located close to helix P4, and R102 is positioned close to helices P3 and P19 of the catalytic domain.

Although P19 is not implicated in a direct interaction with the modeled part of *Zmo*-RnpA, such direct interaction could be mediated by the protein's N-terminal extension, yet its contribution could not be modeled in the absence of an appropriate template and thus remained unexplored. In a recent study, Kazantsev et al.[16] reported the solution structures of three phylogenetically distinct bacterial RNase P RNAs and pinpointed that these ribozymes were described by small ensembles of conformations potentially reflecting their natural flexibility. Thus, depletion of P19 could perturb the structure of the C-domain and its flexibility profile, leading to suboptimal interaction with *Zmo*-RnpA.

To identify structurally and functionally important regions within *Zmo*-RnpA, we screened for conserved positions in other homologous P protein subunits. We focused on the *T. maritima* RNase P protein (*Tma*-RnpA)[15] and calculated the evolutionary rate of each position of the protein subunit using Consurf 2010.[20] Interestingly, as shown in Figure 5C, several amino acids in the P protein of *T. maritima* that are implicated in RNA binding are highly conserved and thus could be functionally important. Although several of these highly conserved residues in *Tma*-RnpA (and *Eco*-RnpA) are also conserved in *Zmo*-RnpA, we could identify several residue alterations that reduced the positive charge of the protein region that is in close contact with helices P2 and P4. For instance, amino acid residues R10, K56, R72, and R73 in *T. maritima* (R11, R57, R74, and L75 in *Eco*-RnpA) are changed to V49, N96, Q112, and S113, respectively, in *Z. mobilis* (Figure 5B). All these positions that are positively charged and assumed to make contacts with catalytically important RPR regions in *T. maritima* and *E. coli* RPR (that lack helix P19) are altered to neutral and uncharged/polar residues in *Z. mobilis*. This could indicate that in the case of *Z. mobilis*, because the protein had co-evolved with the RPR, the additional P19 stem stabilizes the overall fold of the *Zmo* RPR, effectively reducing the necessity of strong electrostatic contacts with the protein for stabilizing the active fold.[22] This is also supported by our results of the heterologous reconstitution experiment, where *Eco*-RnpA,

dx.doi.org/10.1021/bi4011013 | *Biochemistry* 2014, 53, 1810–1817

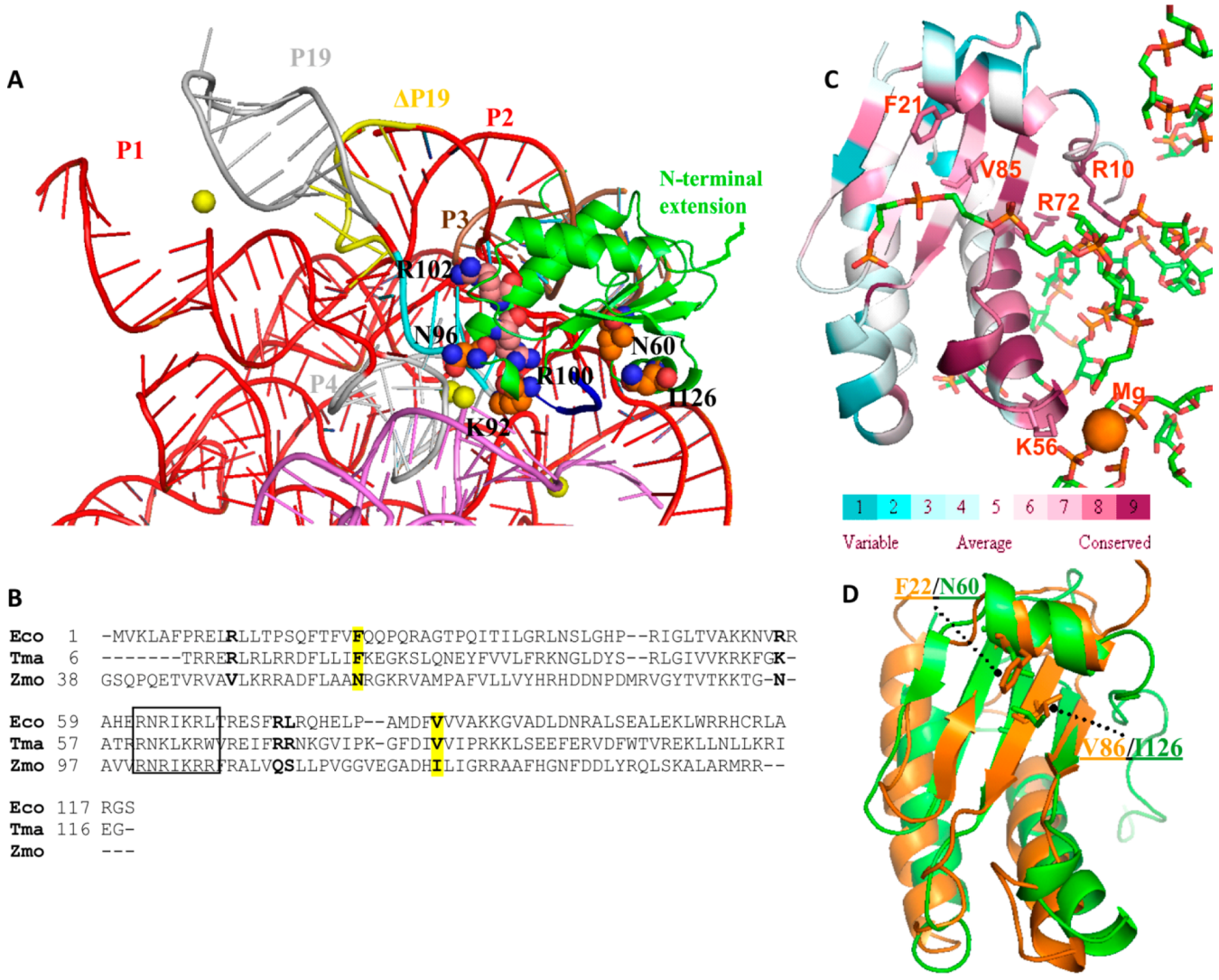

Figure 5. (A) Superposition of the modeled *Z. mobilis* RNase P holoenzyme and the ΔP19 RPR mutant. The P19 stem−loop structure that is present in the native holoenzyme is colored gray, and the four nucleotides at the 3′-end of P2 in the ΔP19 variant (Figure 1) are colored yellow. *Zmo*-RnpA is colored green, and the tRNA is colored magenta. Mg^{2+} ions are colored yellow, and the postcleavage tRNA leader is colored blue. Other residues of the P protein highlighted in the text are also illustrated. The location of the N-terminally extended region of *Zmo*-RnpA that could not be modeled, relative to *Eco*-RnpA, is also illustrated. (B) Alignment of *Zmo*-, *Eco*-, and *Tma*-RnpA (Protein Data Bank entry 3Q1R). Residues implicated in RNA binding are highlighted in bold. Residues highlighted in yellow represent important residue alterations in the central cleft of the *Zmo* protein that could affect the K_m of the protein. The RNR motif residues for the RnpA proteins are displayed with rectangles. (C) ConSurf analysis of *Tma*-RnpA in complex with its cognate RPR binding site and $tRNA^{Phe}$.[15] Amino acids are colored according to their conservation grade using the color-coding bar, with turquoise through magenta indicating variable through conserved, respectively. Only RPR nucleotides within 6 Å of the protein in the X-ray structure of the RNase P holoenzyme are shown. Panel C illustrates highly conserved RnpA residues that are implicated in RNA as well as metal ion binding. This figure was generated using PyMol. (D) Superposition of the *Zmo*-RnpA (green) and *Eco*-RnpA (orange) protein structures along with the residue alterations in the central cleft.

despite the fact that it contains more positively charged residues as described above, ameliorates the *Zmo* RPR activity as much as its cognate protein. Also, *Eco*-RnpA can activate the ΔP19RPR more than its cognate protein. This observation could be due to the elimination of *Zmo*-RnpA-specific RPR contacts by P19 deletion, or *Eco*-RnpA may provide more or stronger side chain contacts to the RPR to better compensate the destabilizing effect of the P19 deletion.

DISCUSSION

In this study, we attempted to investigate the functional role of the P19 element present in a minor fraction of bacterial type A RNase P RNAs. The sequence of the *Zmo* RNase P RNA subunit (RPR) is 69% identical with that of the *E. coli* RPR, and it contains the P19 stem−loop, a highly variable element that is present in many RPR subunits, from different structural classes, but is absent from *E. coli* RPR.[9] These features and the volatile presence of P19 among bacterial RPRs raised the question of its functional role.

To address whether the deletion of P19 could alter RNase P ionic demands, *Zmo* RPR and *Zmo*-RnpA subunits as well as a RPR mutant lacking P19 (ΔP19RPR) were generated and combined to form active reconstituted holoenzymes. The RNase P holoenzyme reconstituted from *Zmo*-RnpA and *Zmo* wtRPR (wtRPR) showed optimal activity at 25 mM $MgCl_2$ and 50 mM NH_4Cl. Elevated magnesium ion requirements for

dx.doi.org/10.1021/bi4011013 | *Biochemistry* 2014, 53, 1810−1817

maximal RNase P catalytic activity have been reported for certain bacteria like *B. subtilis*.[23] Furthermore, the kinetic constants K_m (120 nM) and k_{cat} (4.7 min^{-1}) appear to be in the same range of those reported for RNase P enzymes from other bacteria and eukarya.[24,25] Biochemical characterization of *Zmo* wtRPR and *Zmo* ΔP19RPR in the absence of a protein cofactor revealed temperature and pH optima identical to those of the holoezyme, but monovalent and divalent cation requirements for optimal activity are considerably elevated (Figure 2). P19 seems to be an integral part of the overall fold of the *Zmo* RPR, contributing significantly to the stabilization of the active conformation. This contribution is illustrated by the stark increase in the monovalent cation requirements of the *Zmo* ΔP19RPR for maximal activity, compared to *Zmo* wtRPR. The kinetic analysis revealed a 3.9-fold higher k_{cat} for *Zmo* wtRPR (2.7 min^{-1}) relative to that of *Zmo* ΔP19RPR (0.7 min^{-1}) (Table 1). It is interesting to note that *Zmo* wtRPR has an exceptional G-U wobble pair at the base of P2. This G-U pair may become unstable upon deletion of P19, which could have contributed to the impaired kinetic performance of *Zmo* ΔP19RPR. In conclusion, our results revealed that deletion of the P19 stem−loop does not affect the affinity of the enzyme for the substrate but perturbs the enzyme's catalytic potency, resulting in a substantial reduction of k_{cat}. Moreover, binding experiments of *Zmo* ΔP19RPR or *Zmo* wtRPR with pSupS1 as the substrate (Table 1 and Figure 3) showed that P19 deletion does not alter the substrate binding of RPR. Kinetic analysis of *Zmo* wtRPR and *Zmo* ΔP19RPR revealed identical K_m values, validating the results of electophoretic mobility shift assays (Figure 4). In summary, the approximately 4-fold k_{cat} reduction upon P19 deletion in the RNA-alone reaction is consistent with a role for P19 in folding of the catalytic domain.

Importantly, when we kinetically analyzed *Zmo* ΔP19RPR (resembling *E. coli* and *T. maritima* RPR in terms of the absence of P19) with *Zmo*-RnpA, we observed an increase in constant K_m by a factor of 5.4 (Table 1) compared to that of the native holoenzyme. One possibility is that removal of the P19 hairpin perturbs the structure of the C-domain, leading to suboptimal interaction with *Zmo*-RnpA. To further explore this result, we repeated the kinetics in the presence of the *Eco*-RnpA protein that had co-evolved with the *E. coli* RPR lacking P19. We found that in the presence of *Eco*-RnpA, *Zmo* ΔP19RPR was able to bind the substrate more efficiently [K_m values of 250 and 650 nM for *Zmo* ΔP19RPR and the homologous holoenzyme, respectively (Table 1)]. The observed increased K_m value of *Zmo* ΔP19RPR when combined with *Zmo*-RnpA could also be due to alterations of important residues in the central cleft of *Zmo*-RnpA. The conserved residues F22 and V86 in *Eco*-RnpA (F21 and V85, respectively, in *T. maritima*) are altered to N60 and I126, respectively, in *Zmo*-RnpA (Figure 5B,D). Interestingly, F22 mutations (F22A) in *Eco*-RnpA were shown to dramatically decrease the cleavage activity of *E. coli* RNase P[26] because of the strategic location that F22 holds in the central cleft that binds the 5′-leader sequence of pre-tRNA.[27] To this we could potentially add the alteration of valine (V86) to the larger Ile126 in the central cleft of *Zmo*-RnpA. Indeed, sequence alignment of *Zmo*-RnpA with RnpA proteins from RNase P enzymes that lack P19 revealed that residues N60 and I126 of *Zmo*-RnpA are altered in the other proteins to highly conserved Phe and Val residues, respectively (Figure S3 of the Supporting Information).

Although they belong to the same structural group, *Z. mobilis* RNase P RNA bears an additional P19 stem−loop that is absent from *E. coli* RNase P RNA. Its removal increases the NH_4^+ requirements for RPR optimal activity. The P19 stem−loop is needed to stabilize the interactions with the co-evolved protein within the tertiary fold of the holoenzyme. Further crystallographic studies, in combination with biochemical data, will provide more insights into the role of structural elements of RPRs from different prokaryotes and eukaryotes and the evolution of this diverse holoenzyme.

■ ASSOCIATED CONTENT

Supporting Information

3D structure of the modeled *Z. mobilis* RNase P holoenzyme with wtRPR and ΔP19RPR (Figure S1), electrostatic potential surface of *Z. mobilis* RNase P with wtRPR and *Z. mobilis* RNase P with the ΔP19RPR mutant (Figure S2), sequence alignment of ribonuclease P proteins (Figure S3), cloning of the *Z. mobilis* RNase P RNA subunit (wtRPR) and the mutant ΔP19RRP, and cloning and preparation of the *Z. mobilis* RNase P protein subunit. This material is available free of charge via the Internet at http://pubs.acs.org.

■ AUTHOR INFORMATION

Corresponding Authors

*Department of Biochemistry, School of Medicine, University of Patras, Patras 26504, Greece. Telephone: +302610969127. Fax: +302610969167. E-mail: drainas@med.upatras.gr.

*Department of Biological Applications and Technologies, University of Ioannina, Ipiros, Greece. Telephone: +302651007494. Fax: +302651007064. E-mail: aafendra@cc.uoi.gr.

Present Address

[‖]A.V.: Department of Pathology and Laboratory Medicine, Division of Neuropathology, Perelman School of Medicine, University of Pennsylvania, Philadelphia, PA 19104.

Author Contributions

V.S. and C.T. contributed equally to this work.

Notes

The authors declare no competing financial interest.

■ ACKNOWLEDGMENTS

We thank Dr. Constantinos Stathopoulos (Department of Biological Chemistry, School of Medicine, University of Patras) for critical reading and editing of the manuscript. Dr. Fabrice Jossinet (Institut de Biologie Moleculaire et Cellulaire du CNRS, Université de Strasbourg, Strasbourg, France) is greatly acknowledged for his fruitful assistance with the software assemble for modeling wtRPR.

■ DEDICATION

This work is dedicated to the memory of Professor Constantin Drainas, who lost his life in a car accident on July 5, 2011, while this work was in progress. He is missed greatly.

■ ABBREVIATIONS

RNase P, ribonuclease P; RPR, RNase P RNA; *rnpB*, gene encoding RNase P RNA in bacteria; wt, wild type; ΔP19RPR, *Z. mobilis* RNase P RNA lacking the P19 stem; *Zmo*-RnpA, *Z. mobilis* RNase P protein encoded by the *Zmo-rnpA* gene; pre-tRNA, precursor tRNA; pSupS1, *S. pombe* pre-$tRNA^{Ser}$ gene; PAGE, polyacrylamide gel electrophoresis; SDS, sodium dodecyl sulfate.

REFERENCES

(1) Guerrier-Takada, C., Gardiner, K., Marsh, T., Pace, N., and Altman, S. (1983) The RNA moiety of ribonuclease P is the catalytic subunit of the enzyme. *Cell 35*, 649−857.

(2) Holzmann, J., Frank, P., Löffler, E., Bennett, K. L., Gerner, C., and Rossmanith, W. (2008) RNase P without RNA: Identification and functional reconstitution of the human mitochondrial tRNA processing enzyme. *Cell 135*, 462−474.

(3) Gobert, A., Gutmann, B., Taschner, A., Gössringer, M., Holzmann, J., Hartmann, R. K., Rossmanith, W., and Giegé, P. (2010) A single *Arabidopsis* organellar protein has RNase P activity. *Nat. Struct. Mol. Biol. 17*, 740−744.

(4) Taschner, A., Weber, C., Buzet, A., Hartmann, R. K., Hartig, A., and Rossmanith, W. (2012) Nuclear RNase P of *Trypanosoma brucei*: A single protein in place of the multicomponent RNA-protein complex. *Cell Rep. 2*, 19−25.

(5) Hartmann, E., and Hartmann, R. K. (2003) The enigma of ribonuclease P evolution. *Trends Genet. 19*, 561−569.

(6) Wegscheid, B., Condon, C., and Hartmann, R. K. (2006) Type A and B RNase P RNAs are interchangeable in vivo despite substantial biophysical differences. *EMBO Rep. 7*, 411−417.

(7) Lai, L. B., Chan, P. P., Cozen, A. E., Bernick, D. L., Brown, J. W., Gopalan, V., and Lowe, T. M. (2010) Discovery of a minimal form of RNase P in *Pyrobaculum*. *Proc. Natl. Acad. Sci. U.S.A. 107*, 22493−22498.

(8) Kikovska, E., Wu, S., Mao, G., and Kirsebom, L. A. (2012) Cleavage mediated by the P15 domain of bacterial RNase P RNA. *Nucleic Acids Res. 40*, 2224−2233.

(9) Ellis, J. C., and Brown, J. W. (2009) The RNase P family. *RNA Biol. 6*, 362−369.

(10) Rogers, P. L., Jeon, Y. J., Lee, K. L., and Lawford, H. G. (2007) *Zymomonas mobilis* for fuel ethanol and higher value products. *Adv. Biochem. Eng./Biotechnol. 108*, 263−288.

(11) Christogianni, A., Douka, E., Koukkou, A. I., Hatziloukas, E., and Drainas, C. (2005) Transcriptional analysis of a gene cluster involved in glucose tolerance in *Zymomonas mobilis*: Evidence for an osmoregulated promoter. *J. Bacteriol. 187*, 5179−5188.

(12) Afendra, A. S., and Drainas, C. (1987) Expression and stability of a recombinant plasmid in *Zymomonas mobilis* and *Escherichia coli*. *J. Gen. Microbiol. 133*, 127−134.

(13) Stamatopoulou, V., Toumpeki, C., Tzakos, A., Vourekas, A., and Drainas, D. (2010) Domain architecture of the DRpp29 protein and its interaction with the RNA subunit of *Dictyostelium discoideum* RNase P. *Biochemistry 49*, 10714−10727.

(14) Rother, M., Rother, K., Puton, T., and Bujnicki, J. M. (2011) RNA tertiary structure prediction with ModeRNA. *Briefings Bioinf. 12*, 601−613.

(15) Reiter, N. J., Osterman, A., Torres-Larios, A., Swinger, K. K., Pan, T., and Mondragón, A. (2010) Structure of a bacterial ribonuclease P holoenzyme in complex with tRNA. *Nature 468*, 784−789.

(16) Kazantsev, A. V., Rambo, R. P., Karimpour, S., Santalucia, J., Jr., Tainer, J. A., and Pace, N. R. (2011) Solution structure of RNase P RNA. *RNA 17*, 1159−1171.

(17) Capriotti, E., and Marti-Renom, M. A. (2009) SARA: A server for function annotation of RNA structures. *Nucleic Acids Res. 37*, W260−W265.

(18) Eswar, N., Eramian, D., Webb, B., Shen, M. Y., and Sali, A. (2008) Protein structure modelling with MODELLER. *Methods Mol. Biol. 426*, 145−159.

(19) Koradi, R., Billeter, M., and Wüthrich, K. (1996) MOLMOL: A program for display and analysis of macromolecular structures. *J. Mol. Graphics 14*, 29−32 , 51−55.

(20) Ashkenazy, H., Erez, E., Martz, E., Pupko, T., and Ben-Tal, N. (2010) ConSurf 2010: Calculating evolutionary conservation in sequence and structure of proteins and nucleic acids. *Nucleic Acids Res. 38* (Web Server Issue), W529−W533.

(21) Pappas, K. M., Kouvelis, V. N., Saunders, E., Brettin, T. S., Bruce, D., Detter, C., Balakireva, M., Han, C. S., Savvakis, G., Kyrpides, N. C., and Typas, M. A. (2011) Genome sequence of the ethanol-producing *Zymomonas mobilis* subsp. *mobilis* lectotype strain ATCC 10988. *J. Bacteriol. 193*, 5051−5052.

(22) Buck, A. H., Dalby, A. B., Poole, A. W., Kazantsev, A. V., and Pace, N. R. (2005) Protein activation of a ribozyme: The role of bacterial RNase P protein. *EMBO J. 24*, 3360−3368.

(23) Gardiner, K. J., Marsh, T. L., and Pace, N. R. (1985) Ion dependence of the *Bacillus subtilis* RNase P reaction. *J. Biol. Chem. 260*, 5415−5419.

(24) Vourekas, A., Vryzaki, E., Toumpeki, C., Stamatopoulou, V., Monastirli, A., Tsambaos, D., and Drainas, D. (2009) Partial purification and characterization of RNase P from human peripheral lymphocytes. *Exp. Dermatol. 18*, 130−133.

(25) Toumpeki, C., Vourekas, A., Kalavrizioti, D., Stamatopoulou, V., and Drainas, D. (2008) Activation of bacterial ribonuclease P by macrolides. *Biochemistry 47*, 4112−4118.

(26) Gopalan, V., Baxevanis, A. D., Landsman, D., and Altman, S. (1997) Analysis of the functional role of conserved residues in the protein subunit of ribonuclease P from *Escherichia coli*. *J. Mol. Biol. 267*, 818−829.

(27) Shin, J. S., Kim, K. S., Ryu, K. S., Han, K., Lee, Y., and Choi, B. S. (2012) Structural analysis of *Escherichia coli Eco*-RnpA protein. *Proteins 80*, 963−967.